A complex orthogonal decomposition for wave motion analysis

B.F. Feeny

Department of Mechanical Engineering, Michigan State University, East Lansing, MI 48824, USA,

Abstract

A method is presented for decomposing wave motion into its principle components. The basic idea is a complex generalization of proper orthogonal decomposition. The method involves the representation of real oscillatory signals as complex analytic signals. The relationship between complex modes and wave motion is explored. From an ensemble of complex signals, a complex correlation matrix is formed, and its complex eigensolution is the basis of the decomposition (like a complex singular value decomposition). The complex eigenvectors contain standing and traveling characteristics. A traveling index is proposed to quantify the relative degree of traveling and standing in a waveform. A method of dissecting a wave mode into its traveling and standing parts is also proposed. From the complex modes and modal coordinates, frequencies, wavelengths, and characteristic wave speeds can be obtained. The method is applied to traveling and standing-wave examples.

© 2007 Elsevier Ltd. All rights reserved.

1. Introduction

This paper presents a method of decomposing wave motion into its principle components. The basic idea is a generalization of proper orthogonal decomposition (POD) [1–3]. POD, or similarly Karhunen–Loeve decomposition or principle components analysis, is now a standard tool that has been applied to turbulence, structures, and many other types of systems. For fluids and structures, the POD has been effective at producing modes that optimize the signal energy distribution in a set of measured time series. POD has been applied, for example, to characterize spatial coherence in turbulence and structures [1–7], to evaluate the dimension of the dynamics [3–6,8], to detect modal interactions [9,10], to produce empirical modes for reduced-order models [11–18], and in system identification [19–22]. The POD is also similar to singular value decomposition. All of these tools have been compared for structural applications [23]. The similar biorthogonal decomposition, essentially a singular value decomposition for the application of response ensembles, has also been applied to fluids and plasmas [24,25].

In specific circumstances, the POD produces the normal modes of a structure [26–29], including 2-D structures [30]. The related "smooth decomposition" method can be applied in general cases to find structural modes [31].

E-mail address: feeny@egr.msu.edu

So the POD family of tools is extremely useful, particularly if extracting standing wave components. This paper addresses the decomposition of nonstanding wave components.

The wavelet transform (e.g. Ref. [32]) is another important tool for analyzing wave motion, and is based on localized basis functions, dilated and shifted in time for each signal. It is well suited for multiresolution or time–frequency decomposition of signals [32–36], and obtaining group velocity, dispersion, and attenuation of propagating waves (e.g. Refs. [37–42]), from measurements of a pair of well-spaced sensors. If the wavelet transform were applied to many sensors, as the POD is applied for spatial characterization, and as now the COD is applied, there would be a large dimension of information to process, although still useful for wave decomposition [39]. It can also be done in 2-D [32,36,41].

The approach presented here is a generalization of POD. The basis for discrete POD, in the time-domain perspective, is the real eigen solution of the correlation matrix of the measured ensemble. We generalize this process with the extension of real oscillatory signals to complex phasors. A complex correlation matrix is then formed, and its complex eigensolution is the basis of the decomposition (like a complex singular value decomposition). The complex eigenvectors contain standing and traveling components, which can be identified to produce the full decomposition of traveling and standing waves, whence frequencies and wavelengths can be obtained. In the process, the complex modal coordinates (much like those used for POD [43,44], and equivalently the corresponding components of the bi-orthogonal decomposition [24,25] and the singular value decomposition [45]) can be extracted and used to obtain frequencies and hence characteristic wave speeds.

In the next section, the basic relationship between complex modes and wave motions is examined. This will reveal the motivation for seeking the extension of real signals to the complex phaser representations. Then the decomposition strategy will be laid out and justified. The method will then be applied to examples.

2. Complex modes and wave motions

In this section, we illustrate how a complex modal motion can be interpreted as a combination of traveling and standing waves. We then show how a pure traveling wave can be written as a complex modal motion. That is, *waves are complex modes*.

2.1. Wave interpretation of complex modes

Consider a complex mode of the form $\mathbf{x}_j(t) = e^{\alpha t}\mathbf{u}$, where $\mathbf{x}_j$ is a vector of particle positions, t is time, $\alpha = \gamma + \omega i$, and $\mathbf{u} = \mathbf{c} + \mathbf{d}i$ is a complex mode, with γ, ω, $\mathbf{c}$ and $\mathbf{d}$ being real scalars and vectors. The index j is used to distinguish modes.

Mathematically, $\mathbf{x}_j(t)$ can be considered as a "synchronous complex motion", in the sense that $\mathbf{x}_j = q(t)\mathbf{u}$ is the product of a scalar time function and a fixed vector. However, $\mathbf{x}_j(t)$ does not represent a synchronous motion in its physical interpretation, as not all particles reach the extrema, or zero, simultaneously. These complex modal motions occur in vibration systems with gyroscopic terms or general damping [46,47], or with asymmetric stiffness matrices (flutter).

A linear combination of a complex modal component and its complex conjugate (represented by a bar) is $\mathbf{x}(t) = \mathbf{x}_j(t) + \bar{\mathbf{x}}_j(t) = e^{\gamma t}e^{i\omega t}\mathbf{u} + e^{\gamma t}e^{-i\omega t}\bar{\mathbf{u}} = e^{\gamma t}[(\cos(\omega t) + i\sin(\omega t))(\mathbf{c} + \mathbf{d}i) + (\cos(\omega t) - i\sin(\omega t))(\mathbf{c} - \mathbf{d}i)]$, or

$$\mathbf{x}(t) = 2e^{\gamma t}[\cos(\omega t)\mathbf{c} - \sin(\omega t)\mathbf{d}]. \tag{1}$$

This means that the oscillation has a continual transition from the shape $\mathbf{c}$, when time is in phase with the extremum of the cosine, to the shape $\mathbf{d}$, when time is in phase with the extremum of the sine. The transition from $\mathbf{c}$ to $\mathbf{d}$ is cyclic and ongoing until the exponential decay (for $\gamma < 0$) diminishes the signal to insignificance. This cyclic and ongoing shape transition provides the appearance of a wavy motion if $\mathbf{c}$ and $\mathbf{d}$ are independent. The relative sizes and degree of independence of $\mathbf{c}$ and $\mathbf{d}$ dictate the "amounts" of standing wave and traveling wave components.

Thus the interpretation of a complex modal motion as written above is a motion of frequency ω for each particle, damped exponentially according to γ (if $\gamma < 0$), with a wave speed of $c = \omega/\lambda$, where λ is the wavenumber of $\mathbf{c}$ and $\mathbf{d}$.

2.2. Interpretation of waves as complex modes

Now consider a sinusoidal wave motion of a continuum, for example $y(x, t) = \sin \lambda(x - ct)$. Then

$$y(x, t) = \sin \lambda x \cos \omega t - \cos \lambda x \sin \omega t \tag{2}$$

by using a trigonometric identity, where $\omega = c\lambda$. Then

$$y(x, t) = \text{Re}[e^{i\omega t} \sin \lambda x + i e^{i\omega t} \cos \lambda x] = \text{Re}(z(x, t)), \tag{3}$$

where the complex wave motion $z(x, t) = e^{i\omega t}[\sin \lambda x + i \cos \lambda x]$ perfectly matches the form of a continuous complex mode.

If the continuous structure were sampled at values $x = x_1, x_2, \ldots, x_m$, or if lumped particles were indexed by $i = 1, \ldots, m$, then the discrete parameter complex wave motion would be $\mathbf{z} = e^{i\omega t}[\mathbf{c} + i\mathbf{d}]$ where $\mathbf{c}$ is the spatially sampled $\sin \lambda x$ and $\mathbf{d}$ is the spatially sampled $\cos \lambda x$. Then $\mathbf{z} + \bar{\mathbf{z}}$ would produce a real signal with the interpretation of the previous section.

3. Complex mode decomposition

We first summarize how to express a real oscillatory signal as a complex analytic signal, used in the decomposition process. We then present the decomposition method, justified via an example.

3.1. Complexification of a real oscillatory signal

Our decomposition method is to be applied to complex representations of signals. So real measured signals are first extended to the complex world [48,49]. One way to obtain $z(t)$ uniquely from a real signal $y(t)$ by looking at the Fourier transform $\mathscr{F}(y(t)) = \tilde{Y}(\omega)$, for which there are complex amplitudes associated with frequencies $i\omega_n t$ and $-i\omega_n t$, and truncating the $-i\omega_n t$ from $2\tilde{Y}(\omega)$ to produce $\tilde{Z}(\omega)$. The inverse Fourier transform produces $z(t) = \mathscr{F}^{-1}(\tilde{Z}(\omega))$, which is an analytic signal [48]. More commonly, if $y(t) = \text{Re}(z(t))$, then the Hilbert transform of y is $y_H(t) = \text{Im}(z(t))$ [48,49]. Thus the complex analytic signal [49] is $z(t) = y(t) + i y_H(t)$.

3.2. Complex mode decomposition

This idea is motivated by the POD (time domain perspective), where a correlation matrix is formed. In the proposed work, we generate a complex correlation matrix (of sampled complex signals z_j), and with it, extract complex orthogonal modes in the same manner as POMs are extracted by POD from a real, symmetric correlation matrix. The complex orthogonal modes are then interpreted for their traveling and standing wave components according to the ideas above.

Given the signals, z_j, $j = 1, \ldots, M$, in complex form, where M are the number of sensors distributed on the structure or specimen, we generate vectors $\mathbf{z}_j = [z_j(t_1) \cdots z_j(t_N)]^T$, by sampling at times t_1 through t_N. We build an $M \times N$ complex ensemble matrix $Z = [\mathbf{z}_1 \cdots \mathbf{z}_M]^T$.

Paralleling POD, we construct a complex correlation matrix $\mathbf{R} = (1/N)\mathbf{Z}\bar{\mathbf{Z}}^T$, where the bar indicates complex conjugation. If $\mathbf{Z} = \mathbf{A} + \mathbf{B}i$, then $\mathbf{Z}\bar{\mathbf{Z}}^T = \mathbf{A}\bar{\mathbf{A}}^T + \mathbf{B}\bar{\mathbf{B}}^T + (\mathbf{B}\bar{\mathbf{A}}^T - \mathbf{A}\bar{\mathbf{B}}^T)i$. Since $\mathbf{R} = \bar{\mathbf{R}}^T$ is complex Hermitian, it has real eigenvalues and complex eigenvectors. The complex eigenvectors, $\mathbf{u}_i$, are unique to a scaling constant, which can be complex. (Even when normalized, the unit-magnitude complex scaling constant is not unique.) Furthermore, the Hermitian nature of $\mathbf{R}$ implies that

$$\bar{\mathbf{u}}_i^T \mathbf{u}_j = 0, \quad i \neq j. \tag{4}$$

Due to this orthogonality (unitary) property, we can refer to this method as a complex orthogonal decomposition (COD).

For example, suppose we have a signal with m harmonic wave components, spatially discretized at $x_1, \ldots, x_M$, such that $\mathbf{z}(t) = \sum_{j=1}^{m} q_j(t)\underline{\phi}_j$ is an M vector with m components to be extracted, with

$q_j(t) = (a_j + b_j i)e^{i\omega_j t} = f_j e^{i\omega_j t}$ and $\phi_j(x) = \cos j\lambda x - i \sin j\lambda x$, the samples of which at $x_1, \ldots, x_M$ produce $\underline{\phi}_j$. Then, in matrix form, $\mathbf{z} = \Phi \mathbf{q}$, where $\Phi = [\underline{\phi}_1, \ldots, \underline{\phi}_M]$ is an $M \times M$ modal matrix. The signal is uniformly sampled at times $t = t_1, \ldots, t_N$. As such, the ensemble has the form $\mathbf{Z}_{M \times N} = \Phi_{M \times M} \mathbf{Q}_{M \times N}$.

The complex correlation matrix is then

$$\mathbf{R} = \frac{1}{N}\mathbf{Z}\bar{\mathbf{Z}}^{\mathrm{T}} = \frac{1}{N}\Phi\mathbf{Q}\bar{\mathbf{Q}}^{\mathrm{T}}\bar{\Phi}^{\mathrm{T}} = \Phi\mathbf{R}_Q\bar{\Phi}^{\mathrm{T}},$$

where $\mathbf{R}_Q = (1/N)\mathbf{Q}\bar{\mathbf{Q}}^{\mathrm{T}}$. The elements of $\mathbf{R}_Q$ are

$$r_{Qjk} = \frac{1}{N}\sum_{l=1}^{N} q_j(\omega_j t_l)\bar{q}_k(\omega_k t_l) = \frac{1}{N}\sum_{l=1}^{N} f_j e^{i\omega_j t_l}\bar{f}_k e^{-i\omega_k t_l} = \frac{f_j \bar{f}_k}{N}\sum_{l=1}^{N} e^{i(\omega_j - \omega_k)t_l}.$$

If $\omega_j \neq \omega_k$, then $r_{Qjk} \to 0$ as $N \to \infty$.

Thus, if the frequencies are all distinct, $\mathbf{R}_Q \to \mathbf{D}$ as N gets large, where $\mathbf{D}$ is a diagonal matrix of values $d_j = (1/N)\sum_{l=1}^{N} q_j(t_l)\bar{q}_j(t_l)$. Hence, the matrix $\mathbf{D}$ approaches a diagonal of mean squared *amplitudes* of the complex wave components, as N gets large.

In such case, $\underline{\phi}_j$ are (approximate) eigenvectors of $\mathbf{R}$. To see this, consider

$$\mathbf{R}\underline{\phi}_j \approx \Phi\mathbf{D}\Phi^{\mathrm{T}}\underline{\phi}_j = \Phi\mathbf{D}\mathbf{h}_j,$$

where $\mathbf{h}_j$ is (approximately) a vector of zeros except for the jth element, due to the orthogonality of the complex harmonic basis functions ϕ. (Even if the basis functions are not harmonic but are orthogonal and normalized, then $\mathbf{h}_j$ holds its form.) If $\underline{\phi}_j$ is a discretization of a *normalized* function $\phi_j(x)$, then

$$1 = \int_0^L \phi_j(x)^2 \, \mathrm{d}x \approx \sum_{i=1}^{M} \phi_{ji}^2 \Delta x_i = \Delta x \underline{\phi}_j^{\mathrm{T}} \underline{\phi}_j = \frac{L}{M}\underline{\phi}_j^{\mathrm{T}}\underline{\phi}_j, \tag{5}$$

if $\Delta x_i = \Delta x$ for all i, where ϕ_{ji} is the ith element of $\underline{\phi}_j$, and L is the length of the discretized medium. Thus, the nonzero value in $\mathbf{h}$ will be $\underline{\phi}_j^{\mathrm{T}}\underline{\phi}_j \approx M/L$, the term $\underline{\phi}_j^{\mathrm{T}}\underline{\phi}_j$ representing a rectangular rule approximation of a continuous parameter orthogonality integral in Eq. (5).

Then

$$\mathbf{R}\underline{\phi}_j \approx \Phi\underline{\delta}_j = d_j\underline{\phi}_j M/L,$$

where $\underline{\delta}_j$ is a vector of zeros except for the jth element which is $d_j M/L$. Therefore, $\underline{\phi}_j$ is an approximate eigenvector, and M/L times the mean squared complex modal magnitude, d_j, is the associated eigenvalue, of the complex correlation matrix $\mathbf{R}$. The quality of the approximation depends on the sample resolution, i.e. M and N.

Thus, in the example of complex harmonic waveforms with harmonic modulations, the *COD extracts the complex harmonic waveforms and the mean squared amplitude modulations* through the eigenvalue problem associated with the complex correlation matrix $\mathbf{R}$, yielding eigenvectors and eigenvalues as "complex orthogonal modes" (COMs) and values (COVs). The notion that the COVs are optimal mean squared modal amplitudes is reinforced by the associated Rayleigh's quotient, $\bar{\underline{\phi}}^{\mathrm{T}}\bar{\mathbf{Z}}^{\mathrm{T}}\mathbf{Z}\underline{\phi}/\bar{\underline{\phi}}^{\mathrm{T}}\underline{\phi}$, in which the numerator is the sum of amplitudes of $\mathbf{Z}\underline{\phi}$ elements, which are the complex data projected onto $\underline{\phi}$.

Indeed, as waves are a complex generalization of synchronous motions, this *COD is a generalization of POD*, and will be *able to extract both standing and traveling waves*, as interpreted from the extracted complex modes. Examples will be given shortly.

POD can also recover information about traveling and standing waves. Consider applying POD to a wave of the form of Eq. (2). The POD applied to a discretization of this distributed parameter signal would lead to two POMs, which will represent discretizations of $\sin(x)$ and $\cos(x)$. Further interpretation would be needed to tie these together as components of a single traveling wave. This could be done by using the proper orthogonal modal coordinates (or equivalently, the modal histories that result from singular value decomposition or bi-orthogonal decomposition), and recognizing that these two coordinates have the same frequency and are

$90°$ out of phase. However, the COD will pair these components together, automatically, as real and imaginary parts of a single complex vector. This capability of POD to get equivalent traveling wave components only works when the wave components are orthogonal (purely traveling). We will see an example of this later.

Independently and contemporaneously, Georgiou [50] has applied a complex POD in the frequency domain for response analysis. Direction finding algorithms MUSIC and ESPRIT [51–54] also make use of a complex correlation matrix eigenvalue problem, but with different set-up of data arrays, and different emphasis in the analysis.

3.3. Modal coordinates and wave speed

Similar to writing the complex ensemble as $\mathbf{Z} = \Phi\mathbf{Q}$, we can instead define $\mathbf{Z} = \mathbf{U}\mathbf{Q}_d$, where $\mathbf{U}$ is the matrix of COD orthogonal modes, and $\mathbf{Q}_d$ is the ensemble of complex orthogonal modal coordinates. If the modes in $\mathbf{U}$ are normalized, then by complex orthogonality of Eq. (4),

$$\mathbf{Q}_d = \bar{\mathbf{U}}^{\mathrm{T}}\mathbf{Z}.$$

This is a *complex modal coordinate ensemble matrix*, the rows of which are the samples of each modal coordinate, $q_j(t)$, sampled at $t = t_1, \ldots, t_N$.

The real and imaginary parts of $\mathbf{Q}_d$ provide the two time-modulation components of the complex wave, representing the time modulations of the $90°$-phased components of the wave. Hence, from the modal coordinates in ensemble $\mathbf{Q}_d$, frequency information can be obtained (e.g. by FFT) for the wave components. Likewise, the wavenumber λ_j (2π over the wavelength) can be obtained (by FFT or inspection) from each of the complex modes $\mathbf{u}_j$ from the COD. The wave speed of each wave component is then available, as $c_j = \omega_j/\lambda_j$.

3.4. Traveling and standing waves

The harmonic-wave example used to motivate the decomposition method in Section 3 was a pure traveling wave. However, it is likely that a signal ensemble can represent a combination of traveling and standing waves. Here, we will discuss the quantification of standing and traveling wave components through harmonic examples.

As seen in Section 2, the complex traveling wave can be thought of as a "dance" between configurations defined by the real and imaginary parts of the wave mode, by which the real part is exhibited when the time modulation of the imaginary part is zero, and the imaginary part is exhibited when the time modulation of the real part is zero.

Imagine, for example, that the real part and imaginary part of the complex wave were the same. For a one-mode example, the analog of Eq. (1) is

$$\mathbf{x}(t) = 2\mathrm{e}^{\gamma t}[\cos(\omega t)\mathbf{c} - \sin(\omega t)\mathbf{c}] = 2\mathrm{e}^{\gamma t}[\cos(\omega t) - \sin(\omega t)]\mathbf{c} = 2\sqrt{2}\mathrm{e}^{\gamma t}\cos\left(\omega t - \frac{\pi}{4}\right)\mathbf{c}, \tag{6}$$

which is a standing wave.

Now imagine that the real part were much larger than the imaginary part of the complex wave. The "dance" would take place between a dominant configuration and a diminished configuration, making the dominant configuration appear as almost a standing wave.

More generally, some standing attributes are manifested if the real and imaginary parts of the complex wave mode have something in common, or if they are not the same in magnitude. We propose a "traveling index" defined as the reciprocal of the condition number of the matrix whose two columns are the real and imaginary components of the complex mode. Pure traveling waves will have orthogonal components of the same magnitude, leading to a condition number of 1, and hence a traveling index of one. Deviations, either in the magnitudes of the component vectors, or the directions, will lead to larger condition numbers. Vectors lying in the same direction (completely dependent), or of greatly differing magnitudes, will have large condition numbers, and hence small traveling indices. As the traveling index approaches zero, there is essentially one independent vector, representing purely standing motion.

3.4.1. Standing and traveling addends

We can write the COM vector as $\mathbf{u} = \mathbf{u}_s + \mathbf{u}_t$, where $\mathbf{u}_s$ is a purely standing addend, and $\mathbf{u}_t$ is a purely traveling addend. Then $\mathbf{u}_s = \mathbf{c}_s + i\mathbf{d}_s$ and $\mathbf{u}_t = \mathbf{c}_t + i\mathbf{d}_t$. We aim here to decompose the standing and traveling addends using the ideas above.

Suppose, for example, $\|\mathbf{c}\| \geqslant \|\mathbf{d}\|$. The standing addend of $\mathbf{d}$ is the vector addend that is parallel to $\mathbf{c}$, such that $\mathbf{d}_s = \mathbf{d} \cdot \mathbf{e}_c \mathbf{e}_c$, where $\mathbf{e}_c = \mathbf{c}/\|\mathbf{c}\|$ is the unit vector in the direction of $\mathbf{c}$. Then the traveling vector addend of $\mathbf{d}$ is $\mathbf{d}_t = \mathbf{d} - \mathbf{d}_s$, which is the part that is normal to $\mathbf{c}$. The traveling addend of $\mathbf{c}$ is the piece of $\mathbf{c}$ of the same size as $\mathbf{d}_t$, such that $\mathbf{c}_t = \|\mathbf{d}_t\|\mathbf{e}_c$. Finally, the standing part of $\mathbf{c}_s = \mathbf{c} - \mathbf{c}_t$.

As such, for a single mode motion, or a single-mode reduced motion, with an ensemble such as $\mathbf{Z}_1 = \mathbf{u}\bar{\mathbf{u}}^{\mathrm{T}}\mathbf{Z}$, we would have in continuous time $\mathbf{z}_1(t) = [\mathbf{u}_s + \mathbf{u}_t]q(t) = \mathbf{u}_s q(t) + \mathbf{u}_t q(t) = \mathbf{z}_s(t) + \mathbf{z}_t(t)$. It is easy to show that $\mathbf{z}_s(t)$ is purely standing and $\mathbf{z}_t(t)$ is purely traveling. In this way, a general wave mode can be separated into standing and traveling addends, which can then be examined independently.

3.5. Summary

We have proposed a COD for extracting wave components. The eigenvectors of a complex correlation matrix $\mathbf{R}$ are the complex orthogonal wave modes (COMs), and the eigenvalues (COVs) indicate the mean squared amplitudes of modal wave participation. These COMs contain information about the degree that the motion is traveling. The wavelengths, wave speeds and frequencies can be extracted from the complex modes and modal coordinates. COD is suited for an ensemble, and it involves familiar computations (FFT, correlation and eigensolution).

4. Numerical examples

4.1. A traveling pulse

As an example, we construct a sine-squared pulse wave of length L traveling through a medium of length $L = 8\pi$ (Fig. 1). The continuous waveform is $y(x - ct) = y(h)$, where $h = x - ct$, with $c = L/10 = 4\pi/5$ in this example. Thus, the time taken for the wave to travel through the medium is $T = 10$. The function $y(h)$ is cast in a Fourier series, after which h is replaced with $x - ct$ to represent the traveling wave.

In the Fourier series expansion

$$y(h) = \frac{a_0}{2} + \sum_{n=1}^{\infty}(a_n \cos n\lambda h + b_n \sin n\lambda h), \tag{7}$$

$\lambda = 2\pi/L = \pi/4$, and the Fourier coefficients are $a_0 = 0$, $a_n = -(16/n\pi(n^2 - 16))\sin(n\pi/2)$, $n \neq 4$, and $a_4 = -1/4$, with $b_n = -(16/n\pi(n^2 - 16))(1 - \cos(n\pi/2))$, $n \neq 4$, and $b_4 = 0$. Note that the mean is removed.
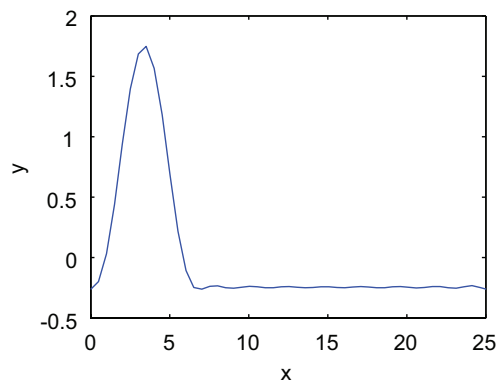

Fig. 1. The pulse waveform, generated by ten Fourier series terms, depicted at $t = 0$. It travels at constant speed to the right, and a new pulse emerges as the first leaves the end of the medium.

The traveling waveform of $y(x - ct)$ is truncated at ten harmonics and then evaluated at 50 equally spaced points from $x = 0$ to L, and sampled at $\Delta t = 0.1$. We used 202 samples instead of a perfectly spatially synchronous 200 samples.

Applying trigonometric identities in the harmonic terms of the $y(x - ct)$ expression of Eq. (7) suggests complex harmonic basis of functions of the form $\cos(n\lambda x) + i\sin(n\lambda x)$, with time modulations $e^{in\omega t - \phi_n}$, where frequency $n\omega = n\lambda c = n\pi/5$.

The wave decomposition was performed on Matlab on this 10-harmonic pulse signal. First the signal $y(x - ct)$ was extrapolated into the complex form using the FFT $-\omega$ truncation method [48]. (This method was chosen at the time of simulation based on familiarity. The Hilbert transform method was applied in subsequent trials with similar results.) The decomposition was done on the complex correlation matrix $\mathbf{R}$ as defined above. The real and imaginary parts of the complex COMs visually match the complex harmonic basis of the $y(x - ct)$ expression of Eq. (7). The first two modes are shown in Fig. 2. There is a slight visual deviation from a pure sinusoid. The traveling indices were computed for each complex mode, and the values for the first nine modes ranged from 0.9753 (fourth mode) to 0.9932 (nineth mode), indicating the numerical error from the constructed traveling index of unity. The tenth mode (ordered by magnitude) is noise, since the eighth harmonic in the pulse wave actually has an amplitude of zero, thereby leading to only nine significant COMs.

Thus, this COD extracted the underlying complex harmonic basis of the Fourier series. The squares of the mean complex amplitudes, $f^2(n) = a_n^2 + b_n^2$ are compared to the eigenvalues, adjusted according to Eq. (5) of the COD, in Fig. 3.
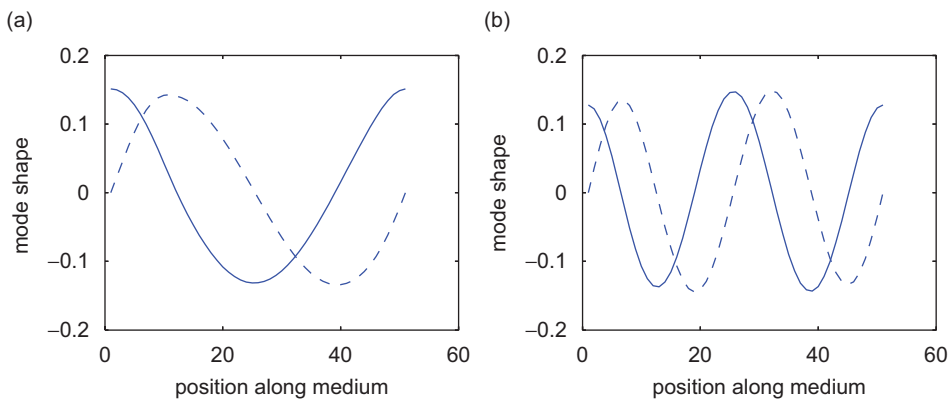

Fig. 2. The real (solid lines) and imaginary parts (dashed lines) of the first two COMs of the traveling pulse: (a) mode 1, and (b) mode 2.
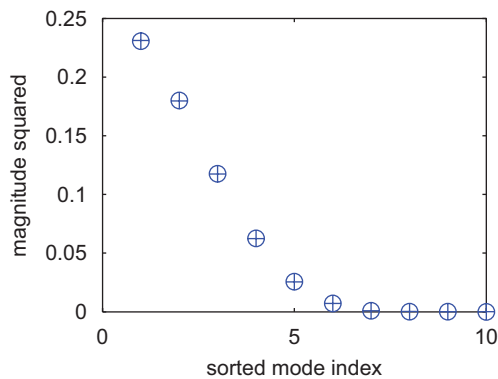

Fig. 3. A comparison between the actual squared modal magnitudes f (○ symbols) and those obtained from the COVs (+ symbols), i.e. the eigenvalues of the associated COMs (after accounting for Eq. (5)) for the traveling pulse.

The wavelengths, by inspection, are L/n, translating to wavenumbers $n\lambda = n/4$. The frequencies of the real parts (or imaginary parts) of the modal coordinates extracted from $\mathbf{Q}_d$ by FFT (or inspection) were multiples of 0.6221, which is very close to $n\omega = n\pi/5$. As such, as constructed, each wave component has the same speed, $c = (n\omega)/(n\lambda) = 0.6221 \times 4 = 2.4884 \approx 4\pi/5$, errors dependent on the synchronicity of the sampling time.

In summary of this example, the COD extracted complex modes that match the orthogonal complex harmonic modes generated from the construction of the waveform via the Fourier series. The Fourier basis is then "optimal," in terms the complex modal coordinate magnitudes, for this waveform. The COD also produced wavenumbers, modal coordinate frequencies, and wave speeds.

4.2. A localized standing wave

In this example we look at a standing wave of the same shape as the pulse examined previously. For the standing wave, $y(x, t) = q(t)\phi(x)$, where $\phi(x)$ has the same form as $y(h)$ in Eq. (7) the previous example, with $\lambda = \pi/2L$, and the same Fourier coefficients as previously. Again, the waveform is constructed with zero mean ($a_0 = 0$). The time modulation function $q(t) = \sin(\omega t)$ is harmonic with frequency $\omega = \pi/5$.

The wave decomposition is performed in Matlab on this 10-harmonic standing signal. The real ensemble is first complexified by the FFT method. The decomposition is again done on the complex correlation matrix $\mathbf{R}$ as defined above. The first two modes are shown in Fig. 4. In this case, only one significant mode results from the COD, and its real part is shaped like the localized wave, while the imaginary part is zero. (The other modes are noisy like mode 2 depicted in Fig. 4.) As such, this mode is enough to represent the dynamics, as it was by construction. The dominant POM is visually identical to real part of the dominant COM, as expected.

By construction, we have a fully standing wave. Fittingly, the traveling index for the significant COM was computed as $2.36e - 17$. In this case, the COD extracted the shape of the dominant standing wave mode, as a single mode, and *did not* extract the underlying complex harmonic basis of the Fourier series. Why? Thinking of the traveling-pulse example, one cannot construct the traveling wave across the whole medium by means of alternating between a real part of that characteristic shape for one phase of the complex harmonic, and an imaginary part of an associated shape for the $90°$ phase of the complex harmonic. In order for the pulse to travel properly with mathematical complex synchronicity, multiple basis functions are needed. However, with the standing wave, there is no alternation between two shapes as the harmonic goes through a $90°$ phase shift. It is indeed possible to set up a synchronous standing wave with a single mode shape. A single tool, the COD, a complex generalization of POD, can sort out the two cases. The real standing wave is represented as a component of the complex wave decomposition. (In this example, it was the real component, but that is an artifact of the phase of our sinusoidal modulation $q(t)$.)
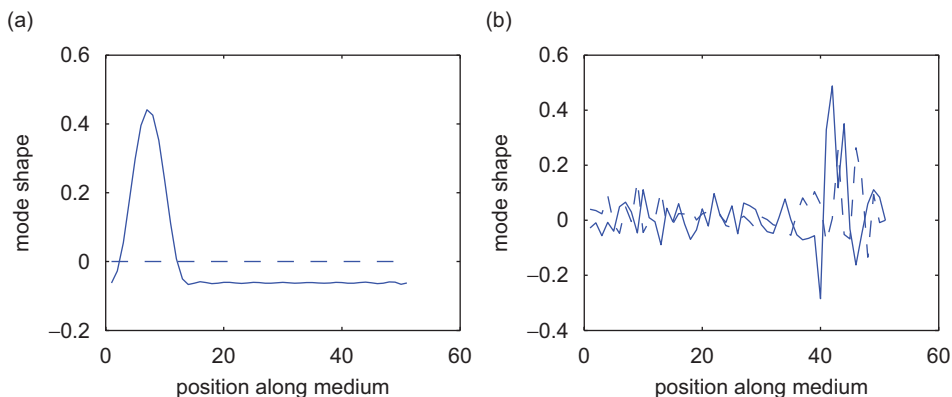

Fig. 4. The real (solid lines) and imaginary (dashed lines) parts of the first two COMs: (a) mode 1, and (b) mode 2.

4.3. Traveling triangle wave

In this example, a wave is constructed not with a harmonic basis, but as a single complex vector $\underline{\phi} = \mathbf{c} + \mathbf{d}i$, where $\mathbf{c}$ and $\mathbf{d}$ are sawtooth functions, out of phase, similar to those shown in Fig. 5. The motion takes place by alternating between the waveforms $\mathbf{c}$ and $\mathbf{d}$, producing a "rolling" effect, in contrast to a sawtooth wave that translates through the medium. As such, this is an example of a waveform that is not constructed via a Fourier series of harmonics.

The COD yields, as the single dominant complex mode (Fig. 5), a vector very close to $\underline{\phi}$.

The constructed wave travels through the wavelength $L = 2\pi$ in 5 s. Thus the wave speed is 1.2566 distance units per second. A comparison of the wave speed for the dominant mode, based on FFT calculations of the first modal coordinate history for its frequency, and the first mode shape for its dominant wavenumber, yields a speed of $\omega\lambda = 1.2566$.

A triangular pulse translating through the medium would be constructed with a Fourier series of harmonic wave components, and like the previous pulse example, would be expected to yield many COMs that match the harmonic wave components.

This example shows that the COD produces COMs that best represent the underlying structure of the waveform. There is no propensity to produce harmonic components, only components that are orthogonal in terms of the Hermitian product.

4.4. Free vibration with general damping

In this final example, we look at a chain of eight unit masses, connected with unit springs, and with at single unit dashpot attached to the end mass. Formulated with the mass displacements as coordinates, the mass matrix is proportional to the identity, the hence modal vectors of the undamped system are mutually orthogonal. In this undamped case, the POD applied to a free vibration with arbitrary initial conditions, or to a response to random excitation, will yield estimates of the normal modes [26–28].

However, with the attached dashpot, the system has nonproportional (non-Rayleigh [55]), and nonmodal (non-Caughey [56]) damping. The damped vibration modes are obtained using the state variable description [46,47]. The equations of motion are

$$\mathbf{M}\ddot{\mathbf{x}} + \mathbf{C}\dot{\mathbf{x}} + \mathbf{K}\mathbf{x} = \mathbf{0}, \tag{8}$$

where $\mathbf{x}$ is an $n \times 1$ array of mass displacements, $\mathbf{M}, \mathbf{C},$ and $\mathbf{K}$, are the $n \times n$ mass, damping, and stiffness matrices, and the dots indicate time derivatives. Then defining a $2n \times 1$ state vector $\mathbf{y}^{\mathrm{T}} = [\dot{\mathbf{x}}^{\mathrm{T}}, \mathbf{x}^{\mathrm{T}}]$, and introducing the equation $\mathbf{M}\dot{\mathbf{x}} - \mathbf{M}\dot{\mathbf{x}} = \mathbf{0}$, yields equations of motion of the form

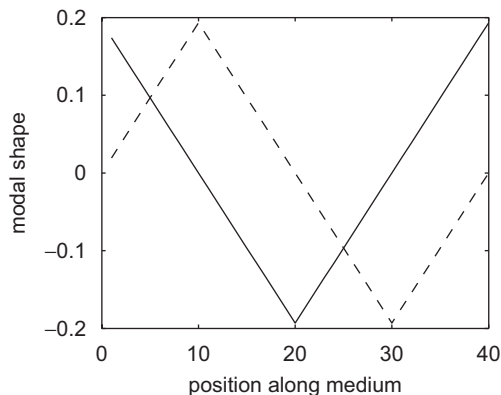$$\mathbf{A}\dot{\mathbf{y}} + \mathbf{B}\mathbf{y} = \mathbf{0}, \tag{9}$$

Fig. 5. The real (solid line) and imaginary (dashed line) parts of a single complex orthogonal mode from a constructed triangle wave.

where $\mathbf{A}$ and $\mathbf{B}$ are $2n \times 2n$ and symmetric, but neither positive nor negative definite. ($\mathbf{A}$ has diagonal $n \times n$ blocks $\mathbf{0}$ and $\mathbf{C}$ and both off-diagonal blocks are $\mathbf{M}$. $\mathbf{B}$ is block diagonal with blocks $-\mathbf{M}$ and $\mathbf{K}$.) Then under the assumption of a response of the form $\mathbf{y} = e^{\alpha t} \underline{\phi}$, the complex modes are obtained from the eigenvalue problem

$$\alpha \mathbf{A} \underline{\phi} + \mathbf{B} \underline{\phi} = \mathbf{0}, \tag{10}$$

which in general yields complex eigenvalues α and eigenvectors $\underline{\phi}$. Now $2n \times 1$ vector $\underline{\phi} = [\mathbf{v}^{\mathrm{T}}, \mathbf{w}^{\mathrm{T}}]^{\mathrm{T}}$, where $\mathbf{v}$ corresponds to characteristic shapes of velocity states, and $\mathbf{w}$ represents characteristic shapes in displacement. By the construction of $\mathbf{y}$, $\mathbf{v} = \alpha \mathbf{w}$. The vectors $\underline{\phi}$ are orthogonal with respect to matrices $\mathbf{A}$ and $\mathbf{B}$. Note, however, that the latter does not imply that the vectors $\mathbf{w}$ are orthogonal with respect to $\mathbf{M}$ and $\mathbf{K}$. In fact, they are not.

For this example, the complex eigenvalues and eigenvectors were obtained, and the free single-complex-mode response was constructed as $\mathbf{x} = e^{\alpha_j t} \mathbf{w}_j + e^{\bar{\alpha}_j t} \bar{\mathbf{w}}_j$, for some $0 < j \leqslant 2n$. In this example, $\alpha_j = -0.2236 \pm 1.2998$, and $\mathbf{w}_j$ is depicted in Fig. 6(a). The imaginary part of α_j indicates a free oscillation frequency and real part indicates the decay rate, or the reciprocal of the time constant. The real and imaginary parts of the mode shape are independent, but not orthogonal. The traveling index was computed as 0.68973, indicating that there is a strong traveling component, but a significant standing component as well.

Fig. 6(b) contains the strobed still image of the free vibration in this mode (animated in Movie 1 of the online version of this paper). From either image, it can be intuitively seen that the motion consists of a combination of standing and traveling components, in that there are no oscillation node points, and the oscillations to and fro do not simply overlap, trusting that indeed the motion is of a single "mode" and not a combination of standing modes.

Applying the COD yielded two "significant" modes, with COVs of 0.0815 and 0.0024. (When the modal motions were made to oscillate without decay, there was only one nonzero COV.) The complex components of the dominant COM are shown in Fig. 7, plotted along with the displacement partition $\mathbf{w}$ of the state-variable linear normal mode $\underline{\phi}$ (solid line). The COM was scaled by a complex nonuniqueness constant to rotate its plot into a comparable orientation. The traveling index computed from the COM was 0.6656, compared to 0.6897 for the displacement partition of the complex normal mode.

For comparison, POD was also applied and it yielded two significant modes, with POVs of 0.0292 and 0.0133. The POMs plotted against each other, analogous to real and imaginary parts, are shown in Fig. 8(a). In this perspective, they qualitatively resemble the normal modes and the COMs, the latter of which is scaled and plotted in a dashed line in Fig. 8(a) for comparison. The POMs are orthonormal by construction, and it turns out that the COMs are nearly orthogonal in this example (not generally the case), but the magnitudes differ. The effect of the differing magnitudes of the complex modes results in the differing magnitudes in the
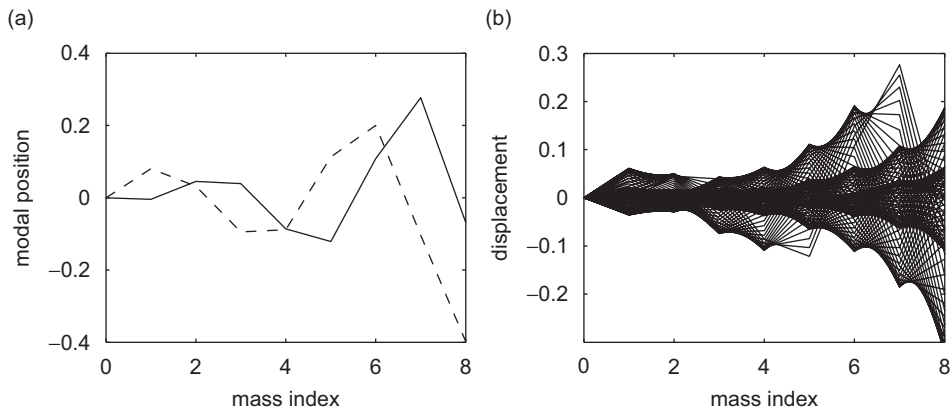

Fig. 6. (a) The displacement partition from a selected state-variable mode shape. The real part is a solid line, and the imaginary part is the broken line. The zero displacement of the wall on the left is incorporated into the modal image. (b) Strobed image of the free-vibration in the selected mode, including the zero displacement of the wall.
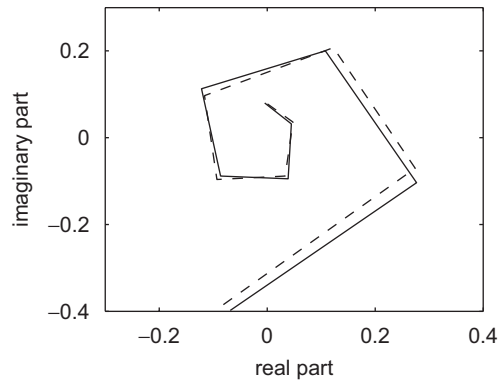
Fig. 7. The dominant complex orthogonal modes (dashed line) and the displacement partition of the state-variable linear normal mode (solid line), in the complex plane.
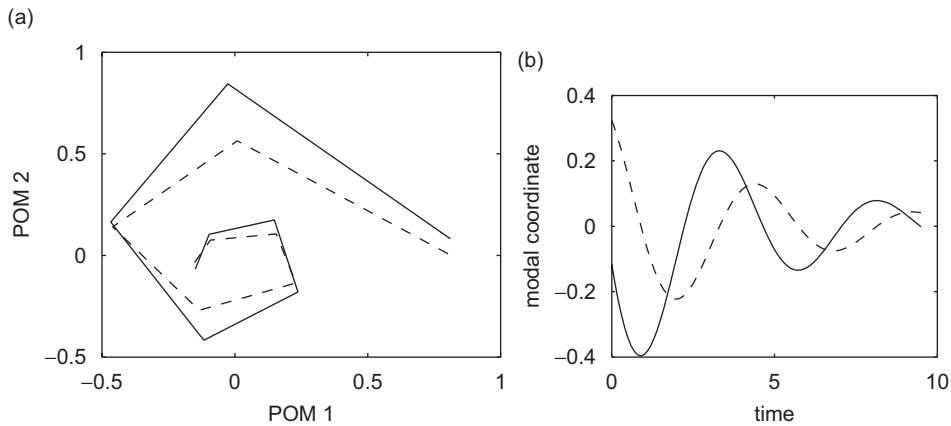

Fig. 8. (a) The first and second proper orthogonal modes plotted against each other (solid line), for each mass index, for comparison with real and imaginary parts of the dominant complex orthogonal mode (dashed line). (b) Proper orthogonal coordinates indicate the phase between the decomposed components. The first (dominant) POC is the solid line, and the second POC is the dashed line.

POCs of Fig. 8(b). The traveling index can be obtained by analyzing the orientation of the POMs and the POCs [57].

We can dissect this modal motion into its standing and traveling addends according to the ideas in Section 3.4.1. The traveling part is shown in Fig. 9(a) (animated in Movie 2 of the online paper), and the standing part is shown in Fig. 9(b) (Movie 3 of the online paper). The last five time samples contained FFT leakage distortions, and were removed. The axes in these images are made the same to provide a visual clue on the relative "amount" of traveling and standing, also sensed in a comparison with Fig. 6(b). The node points of the standing part are clear.

This example shows that the COD produces complex wave components that appropriately represent a physically generated waveform. The traveling index, and traveling and standing addends of the principle wave mode are easily examined. The POD, on the other hand, has restriction that the POMs, representing out of phase modal components, are constrained to be orthonormal.

At the next level of complexity, a multimodal, generally damped free-vibration waveform was also constructed (not shown here). Since the modal vectors $\mathbf{w}_j$ were not mutually orthogonal (as they arose from state modal vectors $\underline{\phi}_j$ that were orthogonal with respect to matrices $\mathbf{A}$ and $\mathbf{B}$), the result of the COD was to generate dominantly three orthogonal complex vectors that did not quite match the true complex structural modal vectors. This is similar to what happens when POD is applied to a signal ensemble generated from nonorthogonal modal components. However, analogous to POD, multimodal COD is expected to be useful
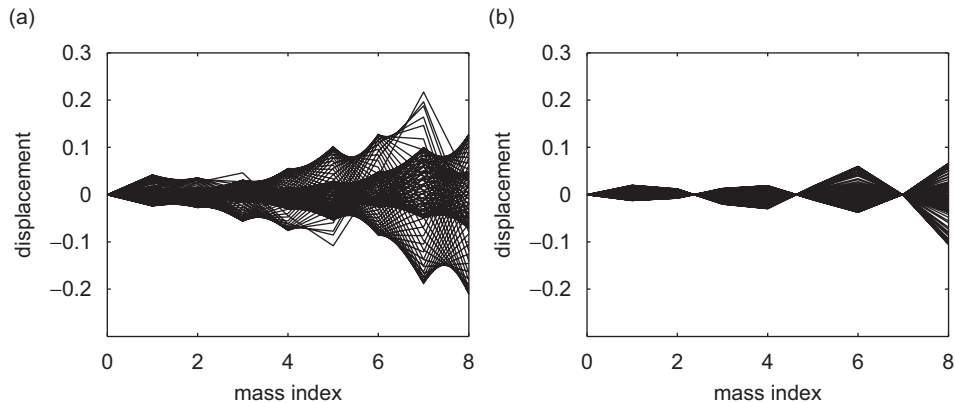
(a)　　　　　　　　　　　　　　　　　　　(b)

Fig. 9. (a) The traveling part of the waveform, (b) the standing part of the waveform.

when the hierarchy of wave mode participation is important, and also in wave studies for which generally damped linear normal modes are not the focus. For multimodal motions, the COD, with real and imaginary parts, has twice the modal capacity as the POD. The detailed features of the multimodal study are interesting, and are the subject of continuing stages of the on-going work.

5. Conclusion

This paper presented a method for extracting oscillatory wave components from an ensemble of dynamic measurements. First, the relationship between complex modes and wave oscillations was explored. Traveling waves can be cast as "complex synchronous modes," and general complex modes can represent a mix of traveling and standing oscillations. A traveling index was proposed to quantify this mix. A method of separating traveling and standing parts was also presented.

The decomposition method is a complex generalization of POD (or similarly singular value decomposition). The wave extraction produces a set of complex orthogonal waves, analogous to the real orthogonal modes of the POD and other methods. The wave components can be analyzed to obtain wavelengths, and the complex principle modal coordinates can be used to obtain modal frequencies, and in turn wave speeds for traveling components.

The method was applied to numerical examples of traveling and standing pulses, and the single-complex-mode free vibration of a multi-degree-of-freedom oscillator with general damping (and complex normal modes). In the oscillator, the decomposed mode was further separated into its traveling and standing parts.

When waves are standing, the method produces the same results as POD. When waves are purely traveling, the method produces the same (and in some cases more) information as POD. But in order for the traveling pairs to be matched in POD, analysis of the proper modal coordinates is needed, while they are automatically paired in the COD, at the light cost of extrapolating the response ensembles into complex analytic signal ensembles. When waves are partially traveling and standing, the COD is more efficient than the POD.

This is the initial study of the method. Future studies may include the robustness to noise, experimental studies and applications, multimodal studies in generally damped systems, gyroscopic systems, or non-structural problems, reduced-order modelling, and the expansion to higher dimensions.

Acknowledgments

Appendix A. Supplementary materials

Supplementary data associated with this article can be found in the online version at doi:10.1016/j.jsv.2007.07.047.

References

[1] J.L. Lumley, The structure of inhomogeneous turbulent flow, in: A.M. Yaglom, V.I. Tatarski (Eds.), *Atmospheric Turbulence and Radio Wave Propagation*, Nauka, Moscow, 1967, pp. 166–178.
[2] J.L. Lumley, *Stochastic Tools in Turbulence*, Academic Press, New York, 1970.
[3] G. Berkooz, P. Holmes, J.L. Lumley, The proper orthogonal decomposition in the analysis of turbulent flows, *Annual Review of Fluid Mechanics* 25 (1993) 539–575.
[4] J.P. Cusumano, B.-Y. Bai, Period-infinity periodic motions, chaos, and spatial coherence in a 10 degree of freedom impact oscillator, *Chaos, Solitons, and Fractals* 3 (5) (1993) 515–535.
[5] J.P. Cusumano, M.T. Sharkady, B.W. Kimble, Spatial coherence measurements of a chaotic flexible-beam impact oscillator, *Aerospace Structures: Nonlinear Dynamics and System Response*, ASME AD-Vol. 33, 1993, pp. 13–22.
[6] B.I. Epureanu, L.S. Tang, M.P. Paidoussis, Exploiting chaotic dynamics for detecting parametric variations in aeroselastic systems, *AIAA Journal* 42 (4) (2004) 728–735.
[7] L. Ukeiley, M. Glauser, D. Wick, Downstream evolution of proper orthogonal decomposition eigenfunctions in a Lobed Mixer, *AIAA Journal* 31 (8) (1993) 1392–1397.
[8] L. Ukeiley, M. Varghese, M. Glauser, D. Valentine, Multifractal analysis of a lobed mixer flowfield utilizing the proper orthogonal decomposition, *AIAA Journal* 30 (5) (1993) 1260–1267.
[9] M.A. Davies, F.C. Moon, Solitons, chaos, and modal interactions in periodic structures, in: A. Guran (Ed.), *Nonlinear Dynamics: The Richard Rand 50th Anniversary Volume*, World Scientific, Singapore, 1997, pp. 119–143.
[10] I.T. Georgiou, I.B. Schwartz, E. Emaci, A. Vakakis, Interaction between slow and fast oscillations in an infinite degree of freedom linear system coupled to a nonlinear subsystem, *Journal of Applied Mechanics* 66 (2) (1999) 448–459.
[11] P. FitzSimons, C. Rui, Determining low dimensional models of distributed systems, in: *Advances in Robust and Nonlinear Control Systems*, ASME DSC-Vol. 53, 1993, pp. 9–15.
[12] G. Kerschen, J.C. Golinval, A.F. Vakakis, L.A. Bergman, The method of proper orthogonal decomposition for dynamical characterization and order reduction of mechanical systems: an overview, *Nonlinear Dynamics* 41 (1–3) (2005) 147–169.
[13] R.V. Kappagantu, B.F. Feeny, Part 2: proper orthogonal modal modeling of a frictionally excited beam, *Nonlinear Dynamics* 23 (1) (2000) 1–11.
[14] R. Kappagantu, B. Feeny, An 'optimal' modal reduction of a system with frictional excitation, *Journal of Sound and Vibration* 224 (5) (1999) 863–877.
[15] B.I. Epureanu, E.H. Dowell, K.C. Hall, Reduced-order models of unsteady transonic viscouls flows in turbomachinery, *Journal of Fluids and Structures* 14 (2000) 1215–1234.
[16] G. Kerschen, B.F. Feeny, J. Golinval, On the exploitation of chaos to produce reduced order models, *Computer Methods in Applied Mechanics and Engineering* 192 (2003) 1785–1795.
[17] M.A.F. Azeez, A.F. Vakakis, Proper orthogonal decomposition (POD) of a class of vibroimpact oscillations, *Journal of Sound and Vibration* 240 (5) (2001) 859–889.
[18] B.I. Epureanu, A parametric analysis of reduced order models of viscous flows in turbomachinery, *Journal of Fluids and Structures* 17 (2003) 971–982.
[19] K. Yasuda, K. Kamiya, Experimental identification technique of nonlinear beams in time domain, *Proceedings of the ASME Design Engineering Technical Conferences*, Sacramento, 1997, on CD-ROM.
[20] X. Ma, A.F. Vakakis, Karhunen-Loève decomposition of the transient dynamics of a multibay truss, *AIAA Journal* 37 (8) (1999) 939–946.
[21] X. Ma, M.A.F. Azeez, A.F. Vakakis, Nonlinear normal modes and nonparametric system identification of nonlinear oscillators, *Mechanical Systems and Signal Processing* 14 (1) (2000) 37–48.
[22] V. Lanaerts, G. Kerschen, J.C. Golinval, Parameter identification of nonlinear mechanical systems using proper orthogonal decomposition, *Proceedings of the International Modal Analysis Conference XVIII*, San Antonio, 2000.
[23] Y.C. Liang, H.P. Lee, S.P. Lim, W.Z. Lin, K.H. Lee, C.G. Wu, Proper orthogonal decomposition and its applications—part 1: theory, *Journal of Sound and Vibration* 252 (3) (2002) 527–544.
[24] N. Aubry, R. Guyonnet, R. Lima, Spatiotemporal analysis of complex signals—theory and applications, *Journal of Statistical Physics* 64 (1991) 683–739.
[25] T.D. Dewit, A.L. Pecquet, J.C. Vallet, The biorthogonal decomposition as a tool for investigation fluctuations in plasmas, *Physics of Plasmas* 1 (10) (1994) 3288–3300.
[26] B.F. Feeny, R. Kappagantu, On the physical interpretation of proper orthogonal modes in vibrations, *Journal of Sound and Vibration* 211 (4) (1998) 607–616.
[27] B.F. Feeny, On the proper orthogonal modes and normal modes of continuous vibration systems, *Journal of Vibration and Acoustics* 124 (1) (2002) 157–160.

[28] B.F. Feeny, Y. Liang, Interpreting proper orthogonal modes in randomly excited vibration systems, *Journal of Sound and Vibration* 265 (5) (2003) 953–966.

[29] G. Kerschen, J.C. Golinval, Physical interpretation of the proper orthogonal modes using the singular value decomposition, *Journal of Sound and Vibration* 249 (5) (2002) 849–865.

[30] U. Iemma, L. Morino, M. Diez, Digital holography and Karhunen–Loeve decomposition for the modal analysis of two-dimensional vibrating structures, *Journal of Sound and Vibration* 291 (1–2) (2006) 107–131.

[31] D. Chelidze, W. Zhou, Smooth orthogonal decomposition-based vibration mode identification, *Journal of Sound and Vibration* 292 (3–5) (2006) 461–473.

[32] D.E. Newland, *An Introduction to Random Vibrations, Spectral and Wavelet Analysis*, third ed., Longman Scientific and Technical, Singapore, 1993.

[33] S.G. Mallat, A Theory for multiresolution signal decomposition—the wavelet representation, *IEEE Transactions on Pattern Analysis and Machine Intelligence* 11 (7) (1989) 674–693.

[34] C.H. Lamarque, S. Pernot, A. Cuer, Damping identification in multi-degree-of-freedom systems via a wavelet-logarithmic decrement—part 1: theory, *Journal of Sound and Vibration* 235 (3) (2000) 361–374.

[35] P. Argoul, T.P. Le, Instantaneous indicators of structural behaviour based on the continuous Cauchy wavelet analysis, *Mechanical Systems and Signal Processing* 17 (1) (2003) 243–250.

[36] D. Coca, S.A. Billings, Continuous-time system identification for linear and nonlinear systems using wavelet decompositions, *International Journal of Bifurcation and Chaos* 7 (1) (1997) 87–96.

[37] K.H. Ip, P.W. Tse, H.Y. Tam, *Extraction of patch-induced Lamb waves using a wavelet transform, Smart Materials and Structures* 13 (4) (2004) 861–872.

[38] F.L. di Scalea, J. McNamara, Wavelet transform for characterizing longitudinal and lateral transient vibrations of railroad tracks, *Research in Nondestructive Evaluation* 15 (2) (2004) 87–98.

[39] A. Roueff, J. Chanussot, J.I. Mars, M.Q. Nguyen, Unsupervised separation of seismic waves using the watershed algorithm on time-scale images, *Geophysical Prospecting* 52 (4) (2004) 287–300.

[40] H.S. Lee, S.H. Kwon, Wave profile measurement by wavelet transform, *Ocean Engineering* 30 (18) (2003) 2313–2328.

[41] M.C. Huang, Wave parameters and functions in wavelet analysis, *Ocean Engineering* 31 (1) (2004) 111–125.

[42] T. Önsay, A.G. Haddow, Wavelet transform analysis of transient wave-propagation in a dispersive medium, *Journal of the Acoustical Society of America* 95 (3) (1994) 1441–1449.

[43] S. Han, B.F. Feeny, Enhanced proper orthogonal decomposition for the modal analysis of homogeneous structures, *Journal of Vibration and Control* 8 (1) (2002) 19–40.

[44] B.F. Feeny, On proper orthogonal coordinates in determining modal activity, *Journal of Sound and Vibration* 255 (5) (2002) 805–817.

[45] G. Kerschen, P. De Boe, J.C. Golinval, K. Worden, Sensor validation using principal component analysis, *Smart Materials and Structures* 14 (1) (2004) 36–42.

[46] L. Meirovitch, *Principles and Techniques in Vibrations*, Prentice-Hall, Upper Saddle River, 1997.

[47] J. Ginsberg, *Mechanical and Structural Vibrations*, Wiley, New York, 2001.

[48] A.V. Oppenheim, R.W. Schafer, *Discrete-Time Signal Processing*, Prentice-Hall, Englewood Cliffs, NJ, 1989.

[49] R.E. Mortensen, *Random Signals and Systems*, Wiley, New York, 1987.

[50] I. Georgiou, Developing POD over the complex plane to form a data processing tool for finite element simulations of steady state structural dynamics, *Proceedings of the International Mechanical Engineering Congress and Exposition*, Chicago, November 5–10, 2006, on DVD-ROM.

[51] R.L. Johnson, An experimental investigation of three eigen DF techniques, *IEEE Transactions on Aerospace and Electronic Systems* 28 (3) (1992) 852–860.

[52] J.W. Pierre, M. Kaveh, Experimental evaluation of high-resolution direction-finding algorithms using a calibrated sensor array testbed, *Digital Signal Processing* 5 (4) (1995) 243–254.

[53] A. Kangas, P. Stoica, T. Soderstrom, Finite-sample and modeling error effects on ESPRIT and MUSIC direction estimators, *IEE Proceedings—Radar Sonar and Navigation* 141 (5) (1994) 249–255.

[54] S.D. Rajan, S.D. Bhatta, Evaluation of MUSIC and ESPRIT algorithms, *Journal of the Acoustical Society of America* 93 (1) (1993) 378–389.

[55] Lord Rayleigh, *The Theory of Sound,* Vol. 1, 1877, reprinted by Dover, New York, 1945, pp. 46–51.

[56] T.K. Caughey, Classical normal modes in damped linear systems, *Journal of Applied Mechanics* 27, Transactions of the ASME 82, Series E, (1960) 269–271.

[57] B.F. Feeny, A method of decomposing wave motions, *Proceedings of the International Mechanical Engineering Congress and Exposition*, Chicago, November 5–10, 2006, on DVD-ROM.